J Mater Sci (2011) 46:6118–6123
DOI 10.1007/s10853-011-5576-7

Three-dimensional fractal analysis of fracture surfaces in titanium–iron particulate reinforced hydroxyapatite composites: relationship between fracture toughness and fractal dimension

Q. Chang · D. L. Chen · H. Q. Ru · X. Y. Yue · L. Yu · C. P. Zhang

Received: 25 November 2010 / Accepted: 19 April 2011 / Published online: 3 May 2011

Abstract Fractal dimension has been considered as a measure of fracture surface roughness of materials. Three-dimensional (3D) surface analysis is anticipated to provide a better evaluation of fracture surface toughness and fractal dimension. The objective of this study was to quantify the fracture surfaces and identify a potential relationship between fracture toughness and fractal dimension in a new type of core–shell titanium–iron particulate reinforced hydroxyapatite matrix composites using SEM stereoscopy coupled with a 3D surface analysis. The obtained results showed that both fracture surface roughness and fractal dimension increased with increasing amount of core–shell Ti–Fe reinforcing particles. The fractal dimension was observed to be a direct measure of fracture surface roughness. The fracture toughness of the composites increased linearly with the square root of fractal dimensional increment (i.e., followed the Mecholsky–Mackin equation well) due to the presence of Ti–Fe particles along with the effect of porosity in brittle materials. The 3D fractal analysis was suggested to be a proper tool for quantifying the fracture surfaces and linking the microstructural parameter to fracture toughness.

Q. Chang · D. L. Chen (✉)
Department of Mechanical and Industrial Engineering, Ryerson University, 350 Victoria Street, Toronto, ON M5B 2K3, Canada
e-mail: dchen@ryerson.ca

Q. Chang · H. Q. Ru · X. Y. Yue · L. Yu · C. P. Zhang
Department of Materials Science and Engineering, School of Materials and Metallurgy, Northeastern University, Wenhua Road 3-11, Shenyang 110004, China

Introduction

Materials science is one of the major fields where quantitative fractography is of vital importance since the mechanical properties of materials are directly associated with the microscopic fracture events or fracture mechanisms/modes. The concept of fractal dimension proposed by Mandelbrot [1],[1] being a measure of the irregular surfaces with self-similar (or self-affine) nature, provides a basis for the quantitative description of tortuosity or roughness/ruggedness of fracture surfaces and other surfaces, and the potential relationship between the fractal dimension and mechanical properties. Coster and Chermant [4], for the first time, pointed out the possibility of applying fractal geometry to the quantitative characterization of fracture surfaces. Manderbrot et al. [5, 6] firstly brought this concept in materials science in 1984, followed by several other Nature and Science articles including [7–10]. Computer models was initially used to simulate a variety of fractal pattern formation processes associated with material failure and deformation, which was found to reproduce surprisingly well the characteristic morphologies observed in a wide range of real material systems, and thus offered a foundation for developing a better understanding of the mechanical properties of materials [10].

Over the last nearly three decades, extensive studies on the applications of fractal geometry in the field of materials science have been conducted on metals [5, 11–20], polymers [21–24], ceramics [25–27], concrete [28], bulk metallic

[1] Dr. Benoît B. Mandelbrot passed away on October 14, 2010, as seen from [2, 3]

glass [29], high-temperature superconductor [30–32], composites [33–36], soft material chocolate [37, 38], trabecular bone [39–41], cells, and rough substrates [18, 42–44]. Recently, a relationship among fractal dimensional increment, fracture energy, Young's modulus, and a characteristic dimension related to the structure of the material has been established to link atomic bond breaking processes to the features on the fracture surface of materials [45]. These studies suggested that the fracture process itself could be of fractal nature and the fractal dimension played a key role in bridging microscopic fracture events and macroscopic properties. So far the fractal dimension has been found extensive applications in many fields. For example, it has been used to study the potential failure causes of clinically ceramic restorations that could not be analyzed only using fractography [46], interpret the relevant experimental data related to the crack-size dependence of the fatigue threshold in metal [47], estimate the theoretical strength so as to assess the potential for improving processing and design of structures [48, 49], offer a new theoretical basis for the empirical Kitagawa diagram used to describe the variation of the fatigue threshold stress intensity range with the crack length [50], establish the relationship between the rupture properties and fracture surfaces in a cobalt-base alloy [51], etc.

It should, however, be noted that the reported experimental results between fractal dimension of fracture surfaces and mechanical properties might be negative [5] or positive [25, 52]. Such relationships have been pointed out to be dependent on the microstructure of fractured materials and measurement methods [13, 53]. For instance, Charkaluk et al. [13] reported that the variations of fractal dimension obtained in some cases could be of the same order of magnitude as the measurement errors. In recent years, a computer-aided stereo matching method using a stereo pair (scanning electron micrographs) has been successfully utilized in the reconstruction and analysis of complex three-dimensional (3D) fracture surfaces in materials [16, 54–59]. This method, which yields the effective depth and shape of the fracture surface features (e.g., pores), permits to overcome the drawbacks and ambiguities of traditional image analysis techniques such as one- (1D) and two-dimensional (2D) measurements, where dark particles often confuse with pores. It is anticipated that the 3D measurements of irregular fracture surfaces with varying scale lengths would be more appropriate to determine the fractal dimension of fracture surfaces.

The present authors [60] have recently developed a new type of titanium–iron particulate reinforced hydroxyapatite composites via pressureless sintering in vacuum at a relatively low temperature. It was observed that the flexural strength, fracture toughness, and fatigue resistance increased significantly with increasing amount of titanium–iron particles due to the occurrence of a variety of toughening mechanisms including crack bridging, branching, and deflection in the composites. The subsequent fracture surfaces looked visibly rougher or more irregular. However, it is unknown if the fractal concept can be used to characterize the fracture surface of the newly developed titanium–iron particulate reinforced hydroxyapatite composites, and if the measuring method of fractal dimension using SEM stereoscopy coupled with 3D surface reported by Venkatesh et al. [16] is able to capture the fracture surface features of brittle materials. Therefore, this study is aimed at evaluating the fractal dimension of fracture surfaces of titanium–iron particulate reinforced hydroxyapatite composites via 3D measurements of fracture surface areas and identifying a potential relationship between the fractal dimension and fracture toughness so as to provide important information on improving the fracture resistance of the bio-composite materials by controlling the microstructural features along with the fabrication process.

Materials and methods

Hydroxyapatite (HA) composites with varying amounts (5, 10, and 15%) of Ti–Fe reinforcing particles with a ratio of Ti–33 wt% Fe were fabricated. Details on the fabrication and processes of the Ti–Fe particulate reinforced HA-matrix composites can be found in our recent publication [60]. The fracture surfaces were obtained from three-point bending (TPB) tests using samples prepared in accordance with ASTM C1161, with a dimension of 25 mm × 2 mm × 2 mm. The tests were conducted with a computerized Instron 8801 testing system in conjunction with a three-point bending stage having a support span of 20 mm. The applied crosshead speed was 0.2 mm/min. Fracture toughness was determined using a Vickers indentation technique [61]. The microstructure and fracture surfaces of the HA-based composites were examined using a scanning electron microscope (SEM) coupled with energy dispersive X-ray spectroscopy (EDS) and 3D fractographic analysis capabilities. Fractal dimensions were determined via the following stages: (1) obtaining 3D images of fracture surfaces by a SEM stereo-imaging technique; (2) converting the 3D images into a digital elevation model (DEM) using a cut-off wavelength of 5λ (where λ is in micrometer) via the MeX software; (3) calculating the fractal dimension and surface roughness. The evaluation method has been described by Venkatesh et al. [16] and is briefly summarized here. The relative area (the ratio of the measured 3D fracture surface area to its projected area) versus the lateral resolution in a double-log coordinate was first plotted [16]. The fractal dimension, D_f, was then evaluated from the slope, k, of the obtained straight line according to the following equation:

$$D_f = 2 - k. \quad (1)$$

The surface roughness was determined from the 3D images of fracture surfaces [62].

$$S_a = \frac{\iint_a |Z(x,y)| dx dy}{A_e}, \quad (2)$$

where $Z(x, y)$ is the height function representing the point-by-point deviations between the measured topography and the mean surface, and A_e is the evaluation area.

In this study, the 3D images of fracture surfaces used for the fractal analysis were taken near the center of fracture surfaces at a magnification of 2000 times. Since the fracture topography itself could affect the final result [15], to improve the accuracy in a statistical sense, five 3D images were analyzed and the averaged values were reported for each composite material.

Results and discussion

The sintering of Ti–Fe particulate reinforced HA-matrix composites in vacuum at 1000 °C for 2 h resulted in a special core/shell structure of Ti–Fe particles that consisted of outer titanium and inner iron [60]. Figure 1 shows a representative back-scattered electron image of the microstructure of HA with 5% Ti–33% Fe particles (taken on a polished sample), together with a typical EDS line scan across the core/shell particle. It is seen that the core/shell type of Ti–Fe particles were uniformly distributed in HA matrix. The presence of titanium located in the outer shell was observed to provide a better interfacial bonding between the HA matrix and reinforcing particles, thus improving the fracture resistance of HA. The details on the formation of the unique core/shell microstructure have been given in [60].

Typical 3D images of fracture surfaces of HA/5%(Ti–33% Fe), HA/10%(Ti–33% Fe), and HA/15%(Ti–33% Fe) are shown in Fig. 2. It is seen from Fig. 2a that the surface of HA with 5% particles exhibited some bumps and ridges. This was attributed to the presence of ductile Ti–Fe reinforcing particles which exhibited plastic stretching due to their relative softness and bridging an advancing crack, thereby making a significant contribution to the improvement of mechanical properties of the composites [60]. Compared Fig. 2b and c with Fig. 2a, it is evident that the bumps and ridges on the fracture surfaces increased considerably with increasing amount of Ti–Fe particles. The above eye-catching observations can further be corroborated by quantitative 3D measurements of the average roughness S_a values obtained from the fracture surfaces of HA composites with 5, 10, and 15% Ti–Fe particles, as shown in Fig. 3. The fractal dimension increased linearly

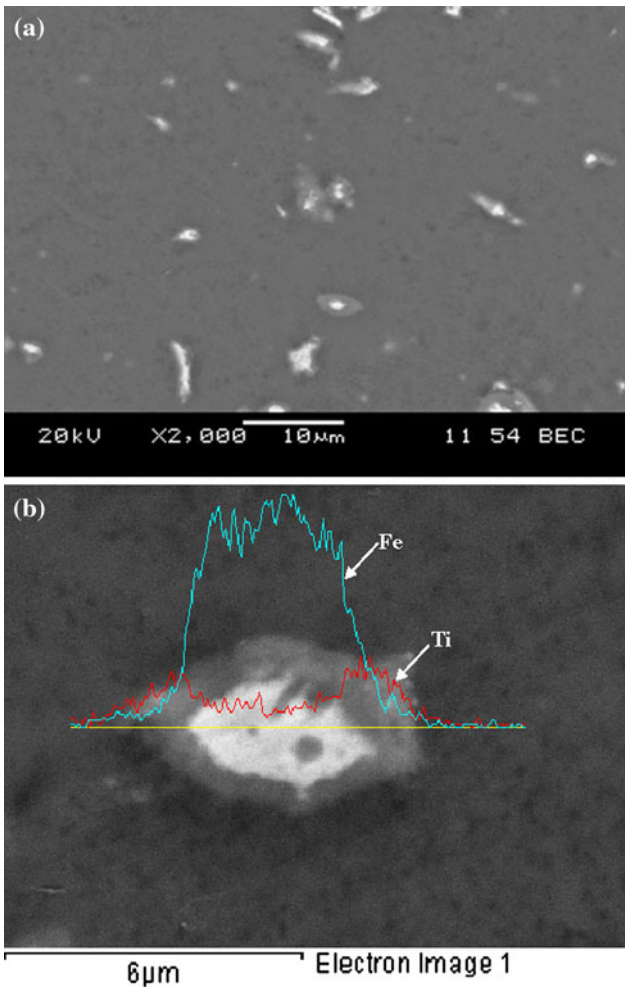

Fig. 1 **a** Back-scattered electron image and **b** EDS line scan across a typical Ti–Fe particle in the HA/5%(Ti–33 wt% Fe) composite

with increasing roughness (and both parameters increased with increasing amount of Ti–Fe particles), which could be described by the following equation,

$$D = \alpha + \beta S_a, \quad (3)$$

$$D^* = \beta S_a, \quad (3a)$$

where $\alpha = 2.00$ and $\beta = 0.16$ in the present study. A similar linear relationship was reported by Venkatesh et al. [16] and Chappard et al. [18] as well. This corresponded well to the fractographs shown in Fig. 2, i.e., the quantitative results were in good agreement with the qualitative appearances of "roughness" or "ruggedness." It follows that the fractal dimension is a direct measure of fracture surface roughness. It should be pointed out that it was not possible to acquire 3D images of the pure HA due to the flatness of its fracture surface [60]. For the sake of discussion below, we assumed that the fracture surface of pure HA was an ideally flat plane with a fractal dimension of 2.00. Furthermore, it has also been recognized the special core–shell Ti–Fe particles were irregular (Fig. 1a), and the

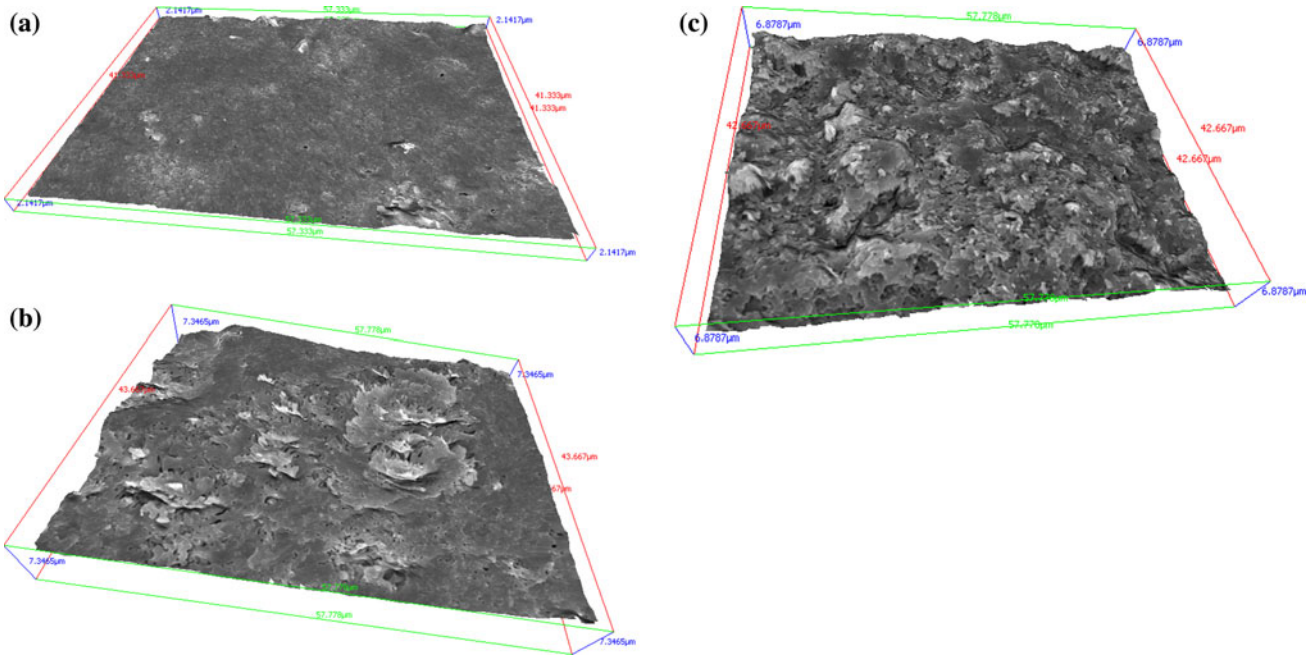

Fig. 2 SEM images of three-dimensional (3D) fracture surfaces for **a** HA/5%(Ti–33 wt% Fe), **b** HA/10%(Ti–33 wt% Fe), and **c** HA/15%(Ti–33 wt% Fe)

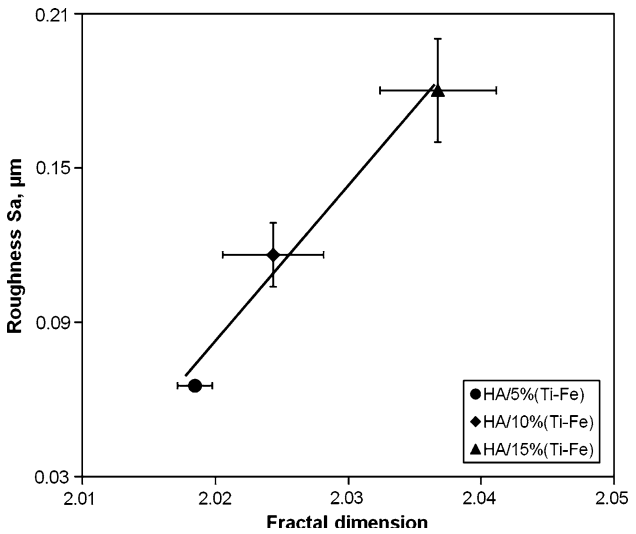

Fig. 3 Average roughness S_a versus fractal dimension of fracture surfaces in the Ti–Fe particulate reinforced HA-matrix composites

interfacial bonding condition between the reinforcing particles and HA matrix would be different. Therefore, the varying extent of the microstructure of the composites increased with increasing content of Ti–Fe particles, which would result in different degrees of fracture topography, accompanied by a bigger scatter of fractal dimension.

The fracture toughness and flexural strength plotted as a function of fractal dimension obtained from the HA-based composites are shown in Fig. 4. It is seen that the fracture toughness increased monotonically with increasing fractal dimension, suggesting a good correlation between the fracture toughness and fractal dimension. This is due to the fact that the fracture toughness is intrinsically associated with the roughness of fracture surfaces that represents the extent of fracture energy absorption or consumption. While the flexural strength also became much higher for the composites caused by the addition of Ti–Fe particles, there was no big change within the experimental scatter. This could be understood from the following relationship among the fracture strength σ_f, fracture toughness K_{IC}, and flaw size a [63],

$$\sigma_f = \frac{K_{IC}}{2}\sqrt{\frac{\pi}{a}}. \quad (4)$$

It can be seen from Eq. 4 that the fracture strength would decrease with increasing flaw size. The initial flaw in the present study could be considered as the pores present in the HA-based composites. The porosity of the composites was observed to increase with increasing amount of Ti–Fe particles [60], thus leading to no further increase in the strength (Fig. 4). However, a certain amount of porosity was reported to have a positive effect on the improvement of toughness in brittle materials via both eliminating the stress concentration of crack tip and closing crack [64] that led to the fracture toughness keeping rising, in spite of its negative effect on the fracture strength.

A relationship between the fracture toughness K_{IC} and fractal dimensional increment D^* for brittle materials has been proposed by Mecholsky and Mackin [65]:

$$K_{IC} = K_0 + E(a_0 D^*)^{1/2}, \quad (5)$$

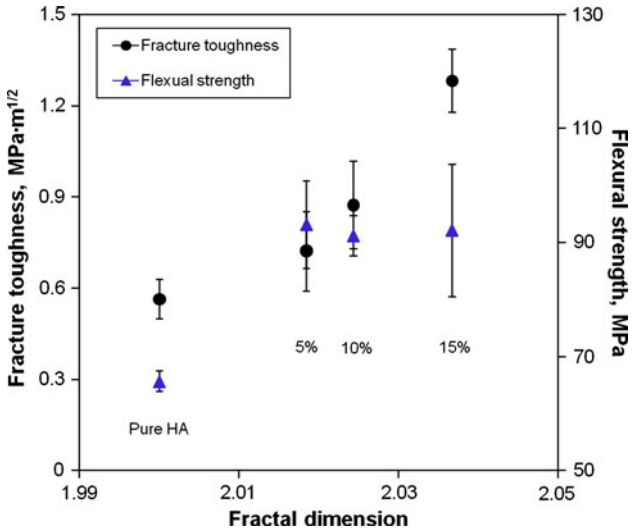

Fig. 4 Variation of fracture toughness and flexural strength with fractal dimension of fracture surfaces in the Ti–Fe particulate reinforced HA-matrix composites

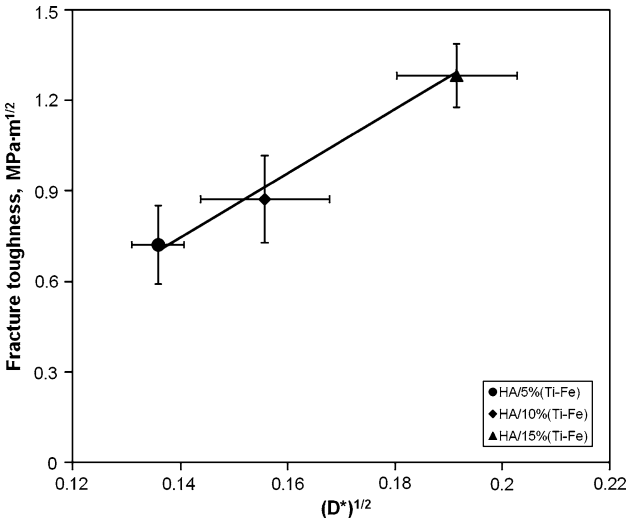

Fig. 5 Fracture toughness as a function of square root of fractal dimensional increment D^* (=$D - 2$) of fracture surfaces in the Ti–Fe particulate reinforced HA-matrix composites

where D^* is the fractional part of the fractal dimension (i.e., $D^* = D - 2$), D is the fractal dimension, E is the Young's modulus, a_o is a characteristic length in the fracture process, and K_o is the toughness value for smooth (Euclidean) planar fracture. The data obtained from the fracture surfaces of HA-based composites with 5, 10, and 15% Ti–Fe particles are plotted in Fig. 5. It is seen that the fracture toughness versus the square root of the fractal dimensional increment followed Eq. 5 well. The results obtained above revealed that the higher the amount of Ti–Fe reinforcing particles, the higher the roughness of fracture surfaces, and the higher the fractal dimension, leading to the higher fracture toughness due to the more energy absorbed. Therefore, fractal dimension offers not only a unique approach for the quantitative description of fracture surface roughness, but also correlates well with the fracture toughness of Ti–Fe particulate reinforced HA-matrix composites.

It should be noted that accurately measuring fracture toughness of brittle materials such as glasses and ceramics is in general challenging, since creating a sharp pre-crack under fatigue loading can be difficult without catastrophically failing the specimen. On the other hand, fracture toughness data using just notched specimens without pre-cracking would have erroneously high values [66, 67]. The indentation technique, being able to be carried out readily without using sophisticated equipment, had arguably been established and could give reasonably consistent fracture toughness values of brittle materials to a certain extent [68–70]. The indentation fracture toughness also allowed a comparison of the performance of manufactured parts since it was reported to be a global value taking into account anisotropy, flaws, interfacial bond, and toughness mechanism [71]. In addition, this technique also found a lot of usage in studying the fracture behavior of ceramic biomaterials and hard tissues [69, 72, 73]. To minimize the uncertainty caused by the crack length measurements [74], the crack lengths were all evaluated under SEM at higher magnifications in the present study. Therefore, the fracture toughness values obtained using Vickers indentation technique were considered to be reasonable. Further studies on the determination of fracture toughness using directly the conventional pre-cracked samples are needed.

Conclusions

The fracture surfaces of a new type of Ti–Fe particulate reinforced hydroxyapatite matrix composites were observed to exhibit basically fractal characteristics. The fractal analysis using SEM stereoscopy coupled with 3D fracture surface measurements revealed a linear relationship between the fractal dimension and fracture surface roughness. The fracture toughness increased significantly after the addition of Ti–Fe particles. While no straightforward relation between the flexural strength and fractal dimension was observed due to the effect of porosity, the fracture toughness increased linearly with the square root of fractal dimensional increment (i.e., followed the Mecholsky–Mackin relationship well) due to the presence of more ductile core–shell Ti–Fe particles and the likely positive effect of porosity on the fracture toughness in the brittle materials. It is thus suggested that the 3D fractal analysis is a suitable tool for quantifying the fracture surfaces and for bridging the microstructural parameter and fracture toughness of ceramic-based composites.

Acknowledgements The authors would like to thank the financial support of Natural Sciences and Engineering Research Council of Canada (NSERC). Q.C. is also to acknowledge the financial support provided by China Scholarship Council and the Fundamental Research Funds for the Central Universities (N090602001) and D.L.C. is also grateful for the financial support by the Premier's Research Excellence Award (PREA), Canada Foundation for Innovation (CFI), and Ryerson Research Chair (RRC) program. The authors would also like to thank Q. Li, A. Machin, J. Amankrah and R. Churaman for their assistance in the experiments. Professor N. Zhang is also gratefully acknowledged for her continuous encouragement while performing this investigation.

References

1. Mandelbrot BB (2000) The fractal geometry of nature, revised edn, 19th printing. W.H. Freeman and Company, New York
2. Gomory R (2010) Nature 468:378
3. Peitgen H-O (2010) Science 330:926
4. Coster M, Chermant JL (1983) Int Metals Rev 28:228
5. Mandelbrot BB, Passoja DE, Paullay AJ (1984) Nature 308:721
6. Mandelbrot BB (2006) Int J Fract 138:13
7. Cahn RW (1989) Nature 338:201
8. Lakes R (1993) Nature 361:511
9. Schaefer DW (1989) Science 243:1023
10. Meakin P (1991) Science 252:226
11. Wang ZG, Chen DL, Jiang XX, Ai SH, Shih CH (1988) Scripta Metall 22:827
12. Williford RE (1990) Scripta Metall Mater 24:455
13. Charkaluk E, Bigerelle M, Iost A (1998) Eng Fract Mech 61:119
14. Yang AM, Xiong YH, Liu L (2001) Sci Technol Adv Mater 2:101
15. Kotowski P (2006) Int J Fract 141:269
16. Venkatesh B, Chen DL, Bhole S (2008) Scripta Mater 59:391
17. Tanaka M, Ono J, Sakashita M, Kato R (2009) ISIJ Int 49:1229
18. Chappard D, Degasne I, Huré G, Legrand E, Audran M, Baslé MF (2003) Biomaterials 24:1399
19. Tanaka M (1995) J Mater Sci 30:3668. doi:10.1007/BF00351883
20. Hilders OA, Ramos M, Pena ND, Saenz L (2006) J Mater Sci 41:5739. doi:10.1007/s10853-006-0102-z
21. Chen CT, Runt J (1989) Polym Commun 30:334
22. Kozlov HV, Burya OI, Aloev VZ (2004) Mater Sci 40:491
23. Du PH, Xue B, Song YH, Lu SJ, Yu J, Zheng Q (2010) Polym Bull 64:185
24. Blacher S, Maquet V, Schils F, Martin D, Schoenen J, Moonen G et al (2003) Biomaterials 24:1033
25. Mecholsky JJ, Passoja DE, Feinberg-Ringel KS (1989) J Am Ceram Soc 72:60
26. Wasen J, Heier E, Hansson T (1998) Scripta Mater 38:953
27. Chen Z, Mecholsky JJ, Joseph T, Beatty CL (1997) J Mater Sci 32:6317. doi:10.1023/A:1018657731971
28. Mechtcherine V (2009) Cem Concr Res 39:620
29. Jiang MQ, Meng JX, Gao JB, Wang XL, Rouxel T, Keryvin V et al (2010) Intermetallics 18:2468
30. Chen DL, Pang DX, Yang ZJ, Kong S, Wang LT, Yang K et al (1988) J Phys C 21:271
31. Fratini M, Poccia N, Ricci A, Campi G, Burghammer M, Aeppli G et al (2010) Nature 466:841
32. Zaanen J (2010) Nature 466:825
33. Rishabh A, Joshi MR, Balani K (2010) J Appl Phys 107:123532. doi:10.1063/1.3445869
34. Liang JZ, Wu CB (2010) Mater Sci Technol 18:178
35. Liang JZ, Wu CB (2009) J Mater Eng 10:53
36. Liang JZ, Wu CB (2008) J Appl Polym Sci 109:3763
37. Cantor GJ, Brown CA (2009) Wear 266:609
38. Briones V, Aguilera JM, Brown C (2006) J Food Eng 77:776
39. Dougherty G, Henebry GM (2001) Med Eng Phys 23:369
40. Wolski M, Podsiadlo P, Stachowiak GW (2009) Proc IMechE H 223:211
41. Majumder SR, Mazumdar S (2007) Physica A 377:559
42. Gentile F, Tirinato L, Battista E, Causa F, Liberale C, di Fabrizio EM et al (2010) Biomaterials 31:7205
43. Wang P, Li L, Zhang C, Lei QF, Fang WJ (2010) Biomaterials 31:6201
44. Borodinsky LN, Fiszman ML (2001) Methods 24:341
45. Mecholsky JJ (2009) Key Eng Mater 409:145
46. Bulpakdi P, Taskonak B, Yan J, Mecholsky JJ (2009) Dental Mater 25:634
47. Carpinteri A, Paggi M (2010) Int J Fract 161:41
48. Mecholsky JJ (2006) Mater Lett 60:2485
49. Carpinteri A, Pugno N, Puzzi S (2009) Chaos Solitons Fractals 39:1210
50. Spagnoli A (2004) Chaos Solitons Fractals 22:589
51. Tanaka M, Kimura Y, Oyama N, Kato R (2006) J Mater Sci 41:6181. doi:10.1007/s10853-006-0176-7
52. Drummond JL, Thompson M, Super BJ (2005) Dental Mater 21:586
53. Della Bona A, Hill TJ, Mecholsky JJ (2001) J Mater Sci 36:2645. doi:10.1023/A:1017948409986
54. Carpinteri A, Chiaia B, Invernizzi S (1999) Theor Appl Fract Mech 31:163
55. Zhou HW, Xie HP (2003) Surf Rev Lett 10:751
56. Tanaka M, Kimura Y, Kayama A, Taguchi J, Kato R (2005) J Mater Sci 40:6291. doi:10.1007/s10853-005-3140-z
57. Ruzicka S, Hausild P (2010) Eng Fract Mech 77:744
58. Adachi K, Chung SH, Friedrich H, Buseck PR (2007) J Geophys Res 112:D14202. doi:10.1029/2006JD8296
59. Elfallagh F, Inkson BJ (2009) J Eur Ceram Soc 29:47
60. Chang Q, Chen DL, Ru HQ, Yue XY, Yu L, Zhang CP (2010) Biomaterials 31:1493
61. Kruzic J, Ritchie RO (2003) J Am Ceram Soc 86:1433
62. ANSI/ASME B46.1-2002, Surface texture (Surface roughness, waviness and lay). American Society of Mechanical Engineers, 2002
63. Kruzic JJ, Satet RL, Hoffmann MJ, Cannon RM, Ritchie RO (2008) J Am Ceram Soc 91:1986
64. Kumar R, Prakash KH, Cheang P, Khor KA (2005) Acta Mater 53:2327
65. Mecholsky JJ, Mackin TJ (1988) J Mater Sci Lett 7:1145
66. Ritchie RO, Dauskardt RH, Yu W, Brendzel AM (1990) J Biomed Mater Res 24:189
67. Fett T, Munz D (2006) Arch Appl Mech 76:667
68. Ponton CB, Rawlings RD (1989) Mater Sci Tech 5:865
69. Scherrer SS, Denry IL, Wiskott HWA (1998) Dental Mater 14:246
70. Kruzic JJ, Ritchie RO (2004) Ceramic Transactions 156:83
71. Gatto A (2006) J Mater Proc Tech 174:67
72. Denry IL, Holloway JA (2004) Dental Mater 20:213
73. Imbeni V, Kruzic JJ, Marshall GW, Marshall SJ, Ritchie RO (2005) Nat Mater 4:229
74. Merkel I, Messerschmidt U (1992) Mater Sci Eng A 151:131